

The flow-field pattern Optimization of the Bipolar Plate for PEMFC Considering the Nonlinear Material

Kap-Seung Choi

Department of Automotive Engineering, Tongmyong University, 428 Sinseon-ro, Nam-gu, Busan, 608-711, Republic of Korea
E-mail: kschoi@tu.ac.kr

Received: 24 November 2014 / Accepted: 28 December 2014 / Published: 19 January 2015

During the assembly of a fuel cell, the mechanical stress and strain that occur have a significantly large effect on the performance and reliability of fuel cell. When assembling a fuel cell stack, the assembly pressure generated can decrease the interfacial contact resistance (ICR) between the bipolar plate (BPP), gas diffusion layer (GDL) and catalyst layer, and also, the reduction in mass transfer that happens during the electrochemical reaction in the catalyst layer through the GDL must be considered. Recent research on the numerical analysis of fuel cells does not take into account the aforementioned importance of the GDL compression deformation, claiming the restrictions of numerical analysis, and uses a simple model to analyze the mass transfer of the fuel cells using CFD analysis. Therefore in this research, the performance of the fuel cell (e.g. pressure drop, gas permeability of GDL, and the electrolyte membrane water content (λ)) were compared for the FSI model, which is a thermal-fluid based PEMFC model (CFD model) that takes the GDL compression deformation into account. The GDL compression deformation, dependent on the fuel cell assembly pressure, affects the gas permeability caused by under-rib convection. As a result in the inlet of the fuel cell, the internal pressure and flow velocity increase due to the decrease in cross sectional area, but due to the decreased gas permeability of the rib it has a low current density, and as the outlet is approached, it can be determined that the current density actually increases due to the hydrogen and oxygen mass fractions being greater than the CFD model making the current density more uniform overall. Therefore using the FSI analysis method, it is important to predict the optimized fuel cell architecture and operating condition parameters.

Keywords: PEMFC(proton exchange membrane fuel cell), Serpentine flow-field design, Optimization, Current density distribution, FSI(Fluid-Structure Interaction), FSI Method

1. INTRODUCTION

A fuel cell is a device that uses hydrogen and oxygen to directly generate electricity, and the uniform supply of hydrogen and oxygen to the entire active area of the fuel cell is important. In a fuel

cell the bipolar plate supplies the O₂ and H₂ necessary for the fuel cell reaction, and also serves the role of a conductor by series connection of the anode and cathode side. Therefore, optimized design of the flow channel, which serves as the conductor and supplies the gases necessary for the reaction, and its height and width are necessary.

The flow pattern of the fuel cell serves an important role in electrochemically distributing the reaction gases to the reaction area of the anode and cathode. Parallel, single serpentine, multiple serpentine, and interdigitated flow patterns are currently being researched, and the multiple serpentine flow pattern shows the best performance [1, 2].

The role of the GDL (Gas diffusion layer), which comes into direct contact with the flow pattern and distributes reaction gases to the catalyst active area, is also important. When assembling a fuel cell stack, the assembly pressure generated can decrease the interfacial contact resistance (ICR) between the bipolar plate (BPP), gas diffusion layer (GDL) and catalyst layer, and also, the reduction in mass transfer that happens during the electrochemical reaction in the catalyst layer through the GDL must be considered. In these two phenomenon, out of the fuel cell stack components, the MEA especially is dependent on its mechanical state. The experimental measurement of the parameters inside the fuel stack is very difficult, and in order to evaluate the mechanical stress and strain of the variable conditions (e.g. clamping load magnitude, stack assembly method, cell design, etc.), finite element analyses (FEA) turned out to be the ideal tool [6].

There is a lot of research using the two methods of FEA and CFD analysis technologies regarding the phenomenon that can occur during the fuel cell stack assembly process that uses a variety of shapes of bipolar plates, which is to mainly increase the performance of the PEMFC [3-11].

Carral et al. [3] verified the number of cells and effects of the parameters dependent on the location of the stack through FEA to examine the interfacial contact resistance (ICR) of the mechanical state of MEA (e.g. MEA Compression ratio, Electrical contact resistance, contact pressure) during the PEMFC stack assembly step. Each MEA mechanical state was shown to be uniform at the 1/2 point of stack (middle point), and as the outer edge was approached, it was reported to show a 3-10% change in uniformity.

Zhou et al. [4] analyzed the effects of the GDL compression deformation on the performance of the PEMFC using the polarization curve obtained from experimental and numerical analysis. The more the contact resistance of the catalyst layer is decreased, the ohmic overpotential of the polarization curve showed a decrease, and the more the GDL compression deformation increased, the porosity variation decreased and the of the reaction gases and of the liquid water decreased. Also, when the GDL compression deformation change was significantly large, it was published that the liquid water saturation increased due to the high current density, high air humidity and the thick catalyst layer.

I. Taymaz and M. Benli [5] reported that the performance of the fuel cell was determined by many parameters, and amongst those parameters, the mechanical deformation due to the assembly pressure affected the contact resistance, porosity and thickness of the GDL. Because excessive assembly pressure destroys the GDL, to obtain high fuel cell performance, it was reported that it is important to combine the FEA model and CFD model to predict the optimum assembly pressure.

As such, the assembly pressure of the fuel cell causes many problems such as fuel leakage, internal combustion, contact resistance, destruction of the MEA and blockage of the gas diffusion passage etc. so there is plenty of research being conducted on these issues using the FEA method.

Also, many researchers through the use of a variety of shapes of bipolar plates, which is to mainly increase the performance of the PEMFC, are conducting research using CFD analysis technology to evaluate the performance of the main parameters, and efficient water management methods inside the channel [1, 12, 13].

Choi et al. [12], in order to investigate the mass transfer (e.g. pressure drop, gas permeability of GDL, and the electrolyte membrane water content (λ) and electro-osmotic drag (α) of the fuel cell, changed the height and width of a 5pass 4turn Serpentine type flow channel, which has a reaction area of 25 cm², and compared the 7-channel shapes. When the height of the channel/rib changed, the reaction area of the channel/rib was the same and there was little improvement to fuel cell performance because the electrochemical reaction due to the mass transfer was the same, but when the width of the channel/rib changed, as the width of the channel increased and the width of the rib decreased, the permeability increased due to under-rib convection, increasing the mass transfer of the bottom of the rib, causing a local increase in current density but due to the low uniformity of the reaction area, it caused a decrease in performance. Also through the control of the flow direction of the under-rib convection, a new shape of channel was proposed and experimentally verified to show a 23% increase in fuel cell performance [13]. In recent research on the numerical analysis of fuel cells, without taking into account the aforementioned importance of the GDL compression deformation, using a simple model that claims the restrictions of numerical analysis, the mass transfer of the fuel cells is being analyzed using CFD analysis. During the fuel cell assembly process, the mechanical stress and changes that occur have a significantly large effect on the performance of the fuel and reliability. Also in the research of Carral et al. [3], because the GDL compression deformation generated at the lamination layer and assembly process causes the electrochemical reaction to be non-uniform, it is advised that the coupled thermal-fluid and solid-mechanics PEMFC model be used for numerical analysis.

This research aims to combine the previously developed thermal-fluid based PEMFC model [12] with the solid-mechanics PEMFC model that takes into account the GDL compression deformation, to investigate the performance of the fuel cell (e.g. pressure drop, gas permeability of GDL, and the electrolyte membrane water content (λ)).

2. MODEL DEVELOPMENT (METHOD)

In this study a 5pass 4turn Serpentine flow field with a fuel cell reaction area of 25 cm² was used [12]. As shown in Fig 1., all the components of the fuel cell are included. A solid model was made using real fuel cell component shape data to make a analysis model for FEA and CFD analysis, and also for FEA, using pressure film, the surface pressure of the boundary and load conditions acting on the fuel cell are measured. Afterwards, the solid model detailed configuration of the boundary and load conditions are set in the FEA program (ABAQUS [14]), and the material characteristics of all the components, such as the Young's modulus and Poisson's ratio etc., are editing into the program, and

the load condition is converted to output voltage (355.125 N) based on the contact stress (1 MPa) for simulation.

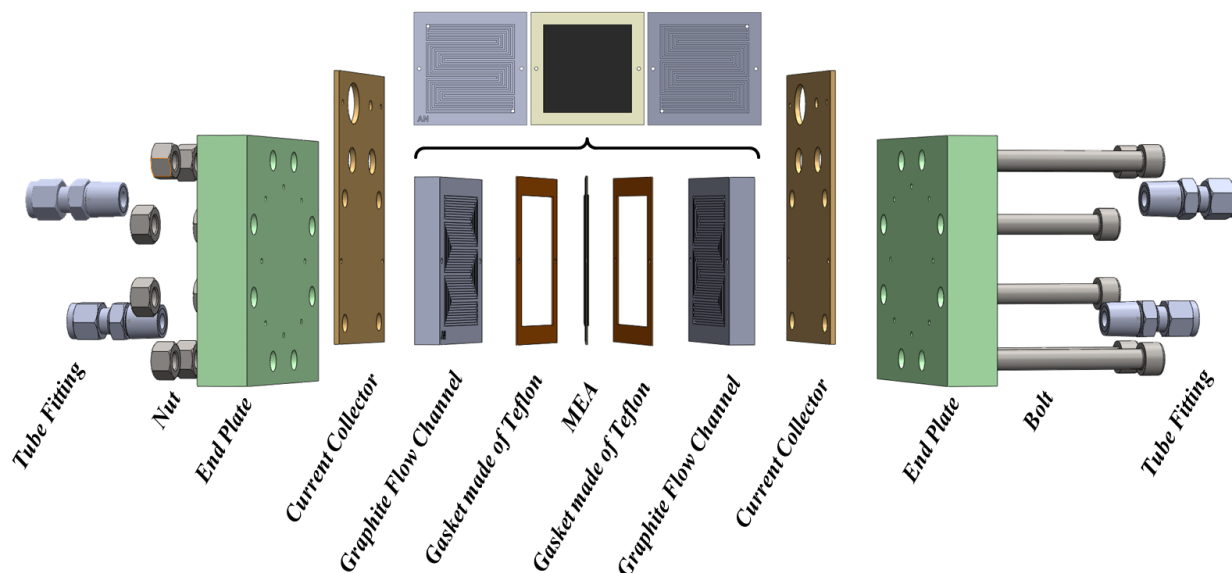


Figure 1. 25 cm² 5pass 4turn Serpentine flow field.

The deformation acting on the MEA is applied as a mesh model contact pressure for each component. The simulation results are shown as mechanical stress, strain, pressure distribution, and deformation etc. of the fuel cell and the changed fuel cell analysis model can be obtained.

To edit the changed FEA model to the CFD model, using the mesh tool (Hyper mesh [15]), the FEA model components can be edited as shown in of Fig. 1(c) to convert to the CFD model. After importing the converted/ edited model to the CFD program (STAR-CD [16]), the boundary conditions, flux, pressure conditions and electrochemical reaction conditions are set and the simulation is run. The important assumptions of the fuel cell CFD analysis are as follows [16].

- Oxygen, Hydrogen, Nitrogen and water etc. are the chemical groups that react in the internal reaction of PEMFC
- Water can be liquid or gaseous, and Nitrogen exists near the MEA.
- The condensation of the water produced by the GDL, and the liquefaction of Hydrogen, Oxygen etc. are modeled as Water film
- Complicated physical phenomenon is calculated using the charge preservation equation etc. for mass, work, energy, chemical groups and electrochemical reactions.
- The analysis of the fuel cell assumes normal state, ideal gas and Homogeneous two phase flow
- The water activity is evaporation/condensation 1.0, and the water that is formed on the surface of the electrolyte in the process of the liquefaction of the gases is assumed to exist as a thin layer state using Henry's Law.

3. RESULTS AND DISCUSSION

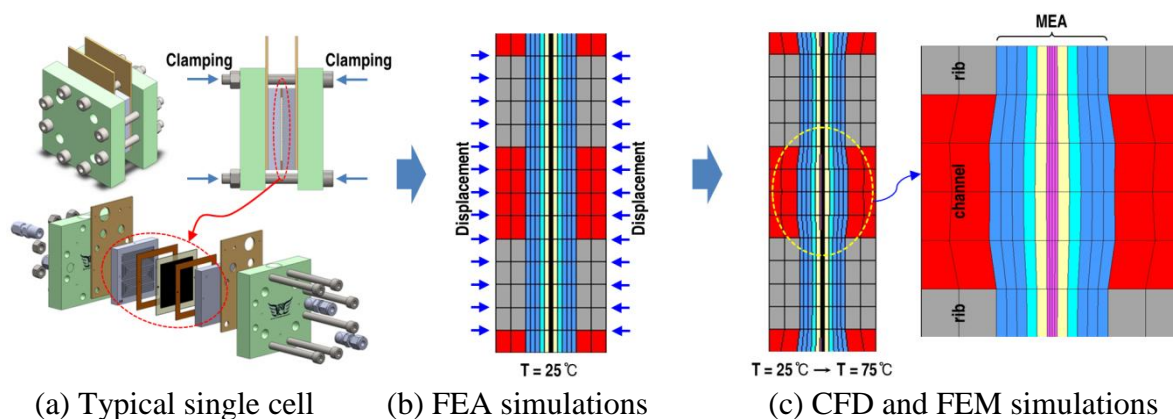


Figure 2. Schematic representations of (a) typical single cell, (b) computational domain for FEA simulations, and (c) computational domain for coupled CFD and FEM simulations

Table 1. Mechanical, thermal, and physical properties

| Parameter | Value | Ref. |
|--|--------------------|---------|
| <i>Bipolar plate(BPP)</i> | | |
| Thermal conductivity (W/m K) | 5.7 | [12] |
| BBP height (mm) | 10 | [12] |
| Channel / Rib / Turn rib width (mm) (w_{ch}) (w_{rib}) (w_{t-rib}) | 1.0 / 1.0 / 1.25 | [12] |
| Channel / Rib / Turn rib height (mm) (h_{ch}) (h_{rib}) (h_{t-rib}) | 0.34 / 0.34 / 0.34 | [12] |
| BBP Young's modulus (MPa) | 13000 | [5, 10] |
| BBP Poisson's ratio | 0.21 | [5, 10] |
| <i>Gas diffusion layer(GDL)</i> | | |
| GDL thickness (mm) | 0.25 | [12] |
| GDL Young's modulus (MPa) | 6.3 | [5, 10] |
| GDL Poisson's ratio | 0.09 | [5, 10] |
| Permeability (m^2) | 1.0e-12 | [12] |
| Diffusion adjustment (%) | 50 | [12] |
| Thermal conductivity (W/m K) | 0.21 | [12] |
| <i>Membrane electrode assembly(MEA)</i> | | |
| MEA thickness (mm) (including 0.0125 mm thickness of catalyst layer) | 0.05 | [12] |
| MEA Young's modulus (MPa) | 63 | [5, 11] |
| MEA Poisson's ratio | 0.1 | [5, 11] |
| Thermal conductivity (W/m K) | 0.15 | [12] |

| | | |
|---|------|------|
| Dry membrane density (g/cm ³) | 2.0 | [12] |
| Equivalent weight of dry membrane (g/mol) | 1100 | [12] |
| Cathode exchange current density (A/cm ²) | 0.02 | [12] |
| Cathode transfer coefficient | 0.6 | [12] |
| Anode exchange current density (A/cm ²) | 0.2 | [12] |
| Anode transfer coefficient | 1.2 | [12] |

As shown in Table 1, the 25 cm² Serpentine flow field is used in the FEM simulation to deduce the results of the GDL compression deformation, and as shown in Table 2, are compared with both the previous results where the operating conditions and the inlet flow velocity were the same [12], and also the results that took into account the GDL compression deformation. As shown in Fig. 3, the analysis results are CFD model (Fig. 3(d)) results that do not take the GDL deformation into account, and through FEA simulation, it is compared with the FSI model (Fig. 3(e)) that takes the GDL compression deformation into account.

The PEMFC performance was analyzed by using the present numerical model of electrochemical reaction and transport phenomena, which are fully coupled using the equations given in references [12], [16].

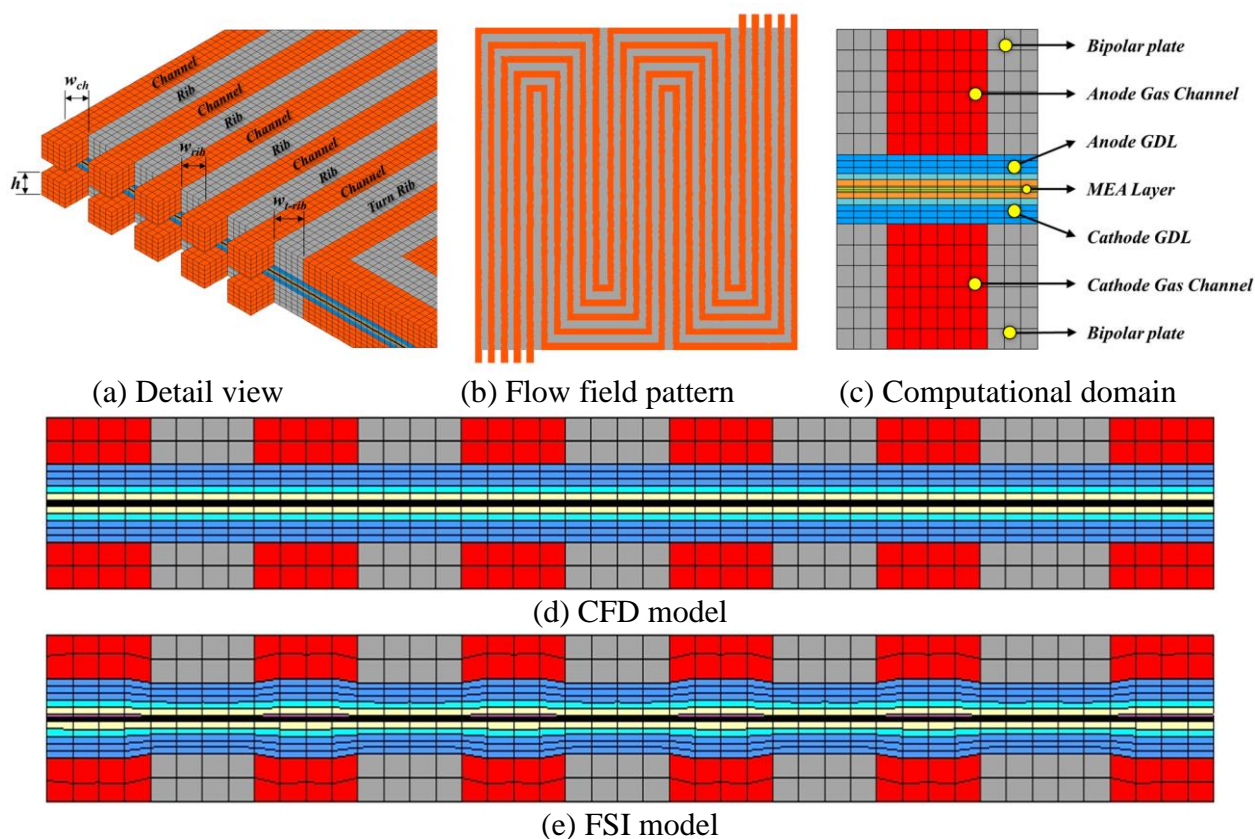


Figure 3. Two 25 cm² serpentine flow-field patterns of 5-passes and 4-turns; (a) Detail view, (b) Flow field pattern, (c) computational domain, (d) CFD model and (e) FSI model.

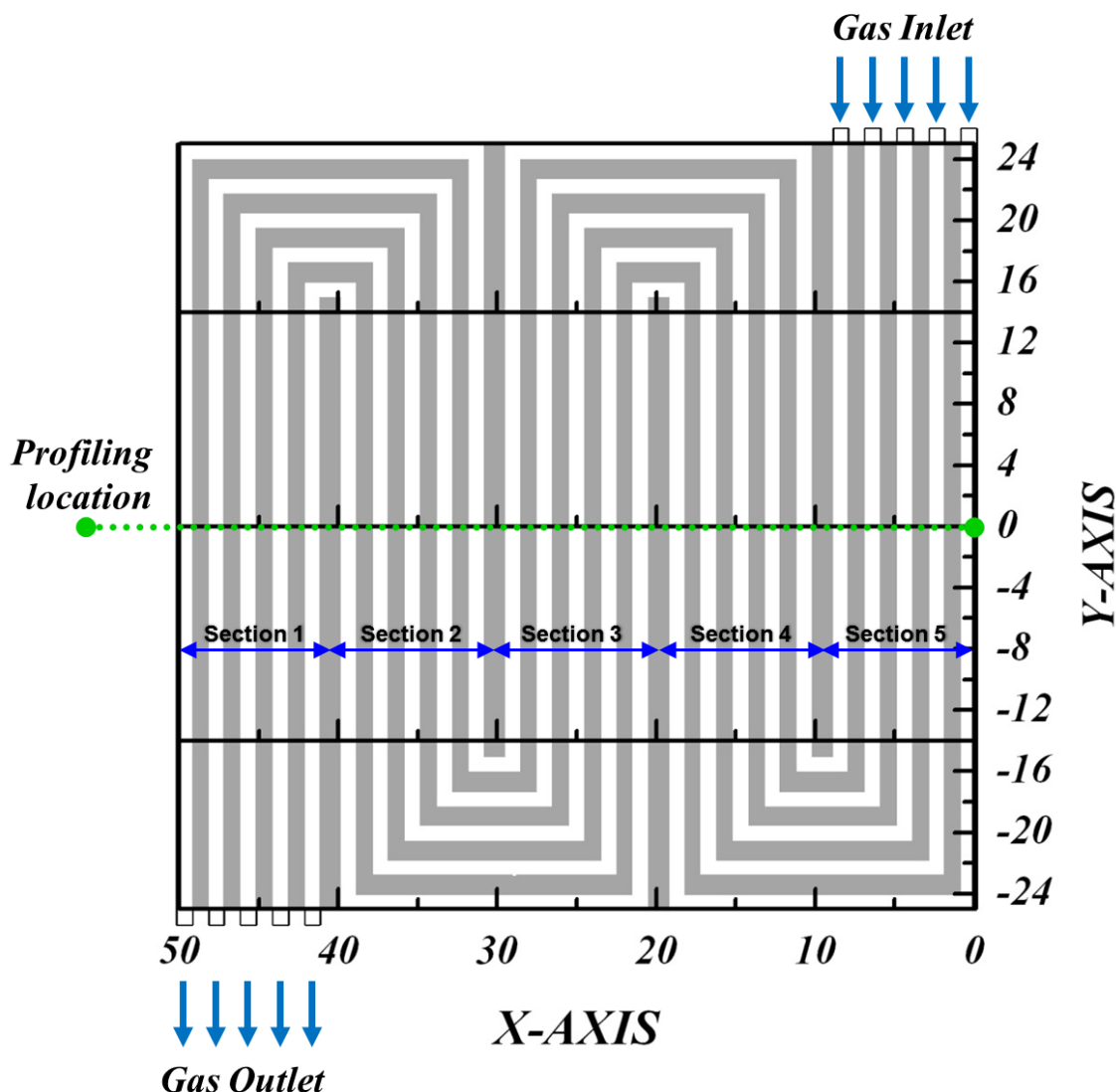
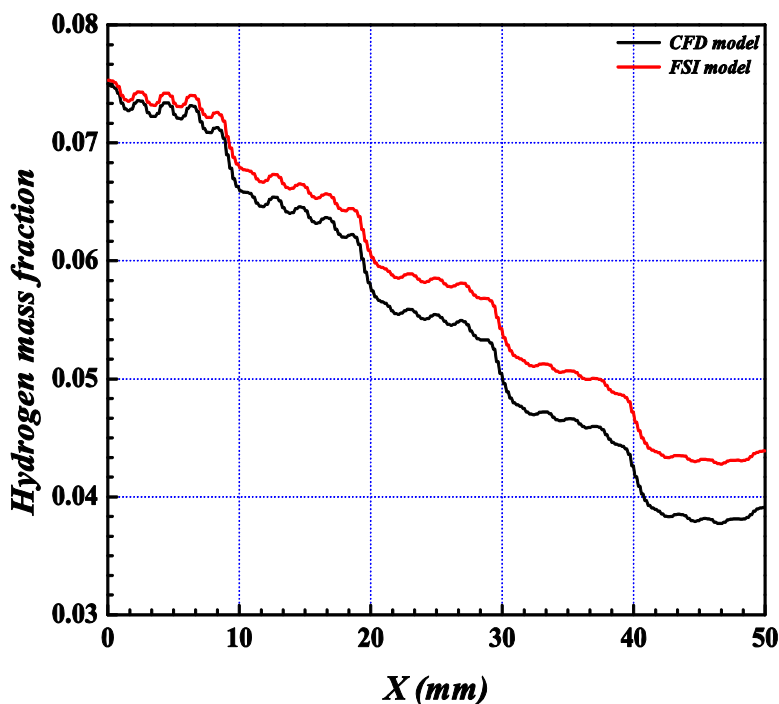
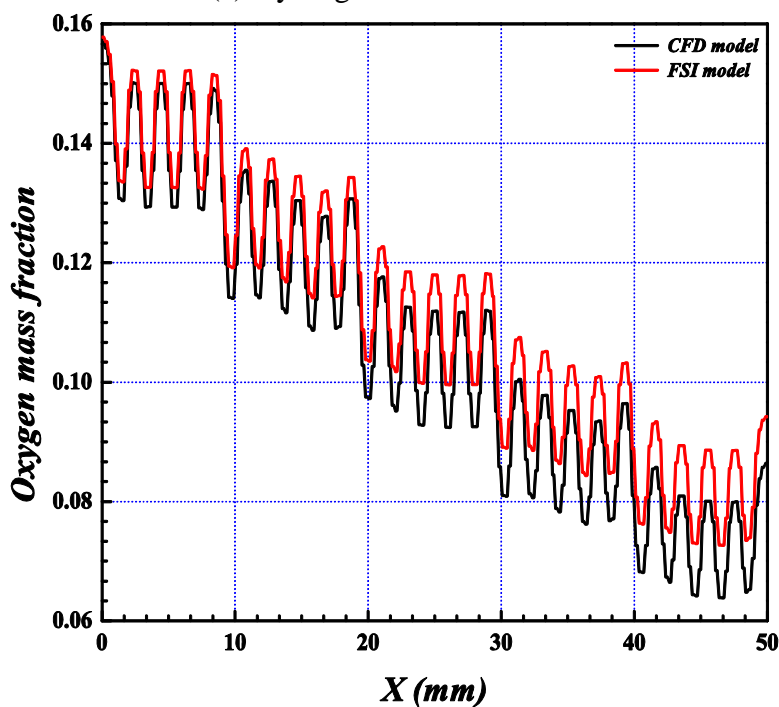


Figure 4. Index and location of the serpentine flow-field for profiling the performance-related parameters.

Therefore, the distributions of performance-related parameters are profiled and compared quantitatively at the same location as shown in Fig. 4. The performance-related parameters include the hydrogen and oxygen mass fraction, membrane water content (λ), net water flux per proton (α), liquid water mass fraction, total pressure, current density distributions, and polarization and power density curves. In the case of the FSI model, GDL compression deformation was generated due to the assembly pressure. Most of the GDL deformation, because the width of the channel and rib are within 1 mm, was in the form of expansion on the channel and there was compression in the rib and turn rib. Fig. 5-9 shows these results and how the GDL deformation affects the internal performance using the average current density (I_{avg}) 0.6 A/cm^2 .



(a) Hydrogen mass fractions



(b) Oxygen mass fractions

Figure 5. Hydrogen mass fractions and oxygen mass fractions in CFD model are compared with those in FSI model at $I_{ave} = 0.6 \text{ A/cm}^2$.

Fig. 5 shows the mass fraction of hydrogen and oxygen. As shown in Table 2, when the stoichiometric ratio was 1.5/2.0, the concentration change showed a decrease from the inlet to the outlet, and shows a similar tendency to the internal pressure of the fuel cell in Fig. 6. This is due to under-rib convection, and in the case of the FSI model, the GDL thickness of the rib was compressed

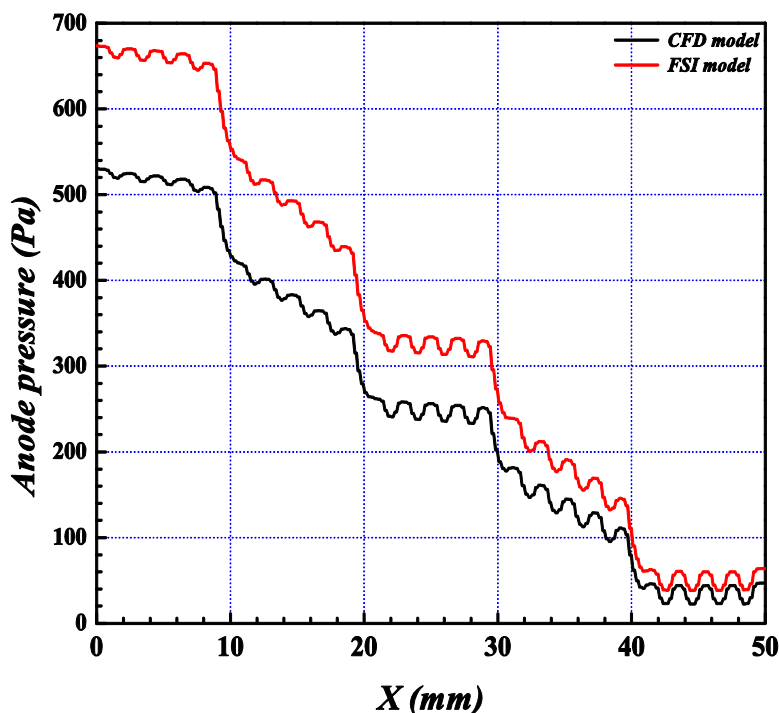
causing the permeability of the gas to decrease, and it showed that in comparison to the CFD model, the concentration was high.

Table 2. Operating conditions

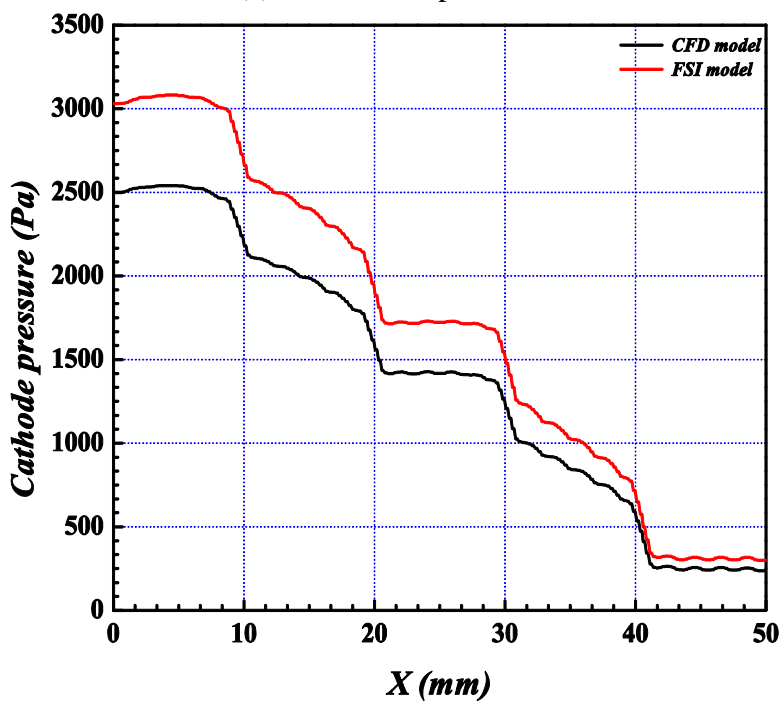
| | Inlet conditions |
|---|------------------|
| <i>Anode</i> | |
| Gas | Hydrogen |
| Stoichiometry | 1.5 |
| Inlet temperature(°C) | 75 |
| Inlet relative humidity(%) | 100 |
| Mass fraction of hydrogen | 0.078 |
| Mass fraction of Water | 0.561 |
| <i>Cathode</i> | |
| Gas | Air |
| Stoichiometry | 2.0 |
| Inlet temperature(°C) | 75 |
| Inlet relative humidity(%) | 100 |
| Mass fraction of Oxygen | 0.169 |
| Mass fraction of Water | 0.274 |
| <i>Operating conditions</i> | |
| %H ₂ in reformat | 75 |
| Exit pressure(kPa) | 101 |
| H ₂ exchange current density(A/cm ²) | 2000 |
| O ₂ exchange current density(A/cm ²) | 200 |
| Open circuit voltage(V) | 0.96 |
| Cell temperature(°C) | 75 |

Also, the mass transfer and electrochemical reactions etc. of the PEMFC occurred through convection and diffusion, and the main mass transfer method was convection. The mass transfer rate and gas permeability in the inside of the GDL were usually determined by the pressure difference in the adjacent channels.

The main cause of the increase in the mass fraction of the FSI model, as shown in Fig. 5, is the GDL deformation. The GDL deformation, which is a 7.18% (0.0012 cm²) reduction in cross-sectional area in the channel and a 9.92% (24.8 μm) reduction of thickness in the z-direction of the rib, is caused by the decrease in gas permeability by under-rib convection.



(a) Anode total pressure

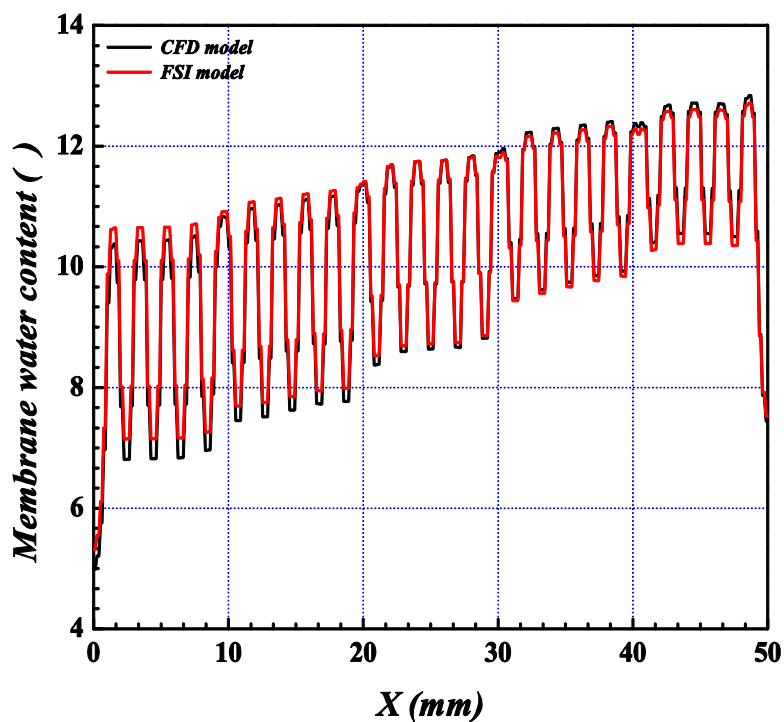


(b) Cathode total pressure

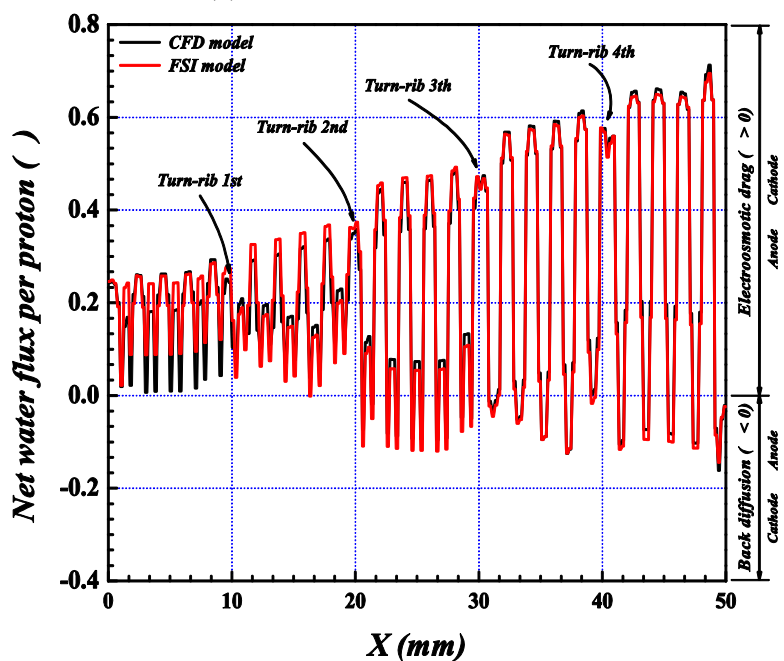
Figure 6. Total pressure on the anode and cathode side in CFD model are compared with those in FSI model at $I_{ave} = 0.6 \text{ A/cm}^2$.

Fig. 6 shows a comparison between the total pressure of the anode and cathode for the CFD model and FSI model. The total pressure of the anode and cathode continuously decreases from the inlet until the outlet is reached, and it decreases dramatically in the turn-rib. This is caused by frictional and bending losses in the serpentine flow field pattern. The reason the FSI model shows a higher

pressure than the CFD model is largely due to the effect of the reduction of cross-sectional area and the compression of the turn GDL of the rib.



(a) Membrane water contents



(b) Net water flux per protons

Figure 7. Membrane water contents and net water flux per protons in CFD model are compared with those in FSI model at $I_{ave} = 0.6 \text{ A/cm}^2$.

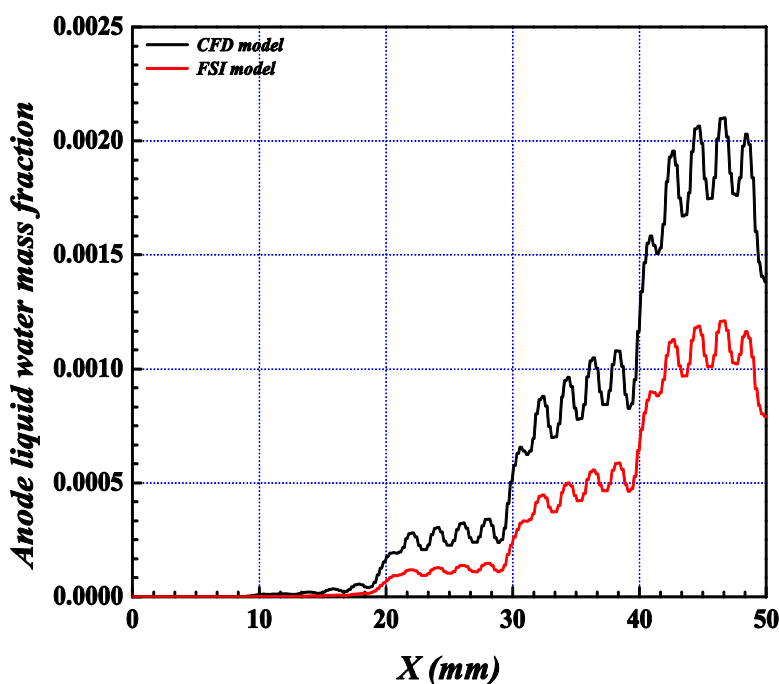
Because the membrane water content (λ) is dependent on the total pressure, the liquid water of the fuel cell exists in liquid phase and vapor phase due to the partial pressure and total pressure of

water vapor, and is shown in Fig. 7. For the membrane water content (λ), because the amount of water flowing in the direction of the flow channel increases to show a low membrane water content (λ), a larger amount of water is absorbed into the electrolyte membrane due to the high flow rate between the GDL and rib caused by the under-rib convection of the rib than the amount of water absorbed into the electrolyte membrane due to the high pressure at the inlet channel.

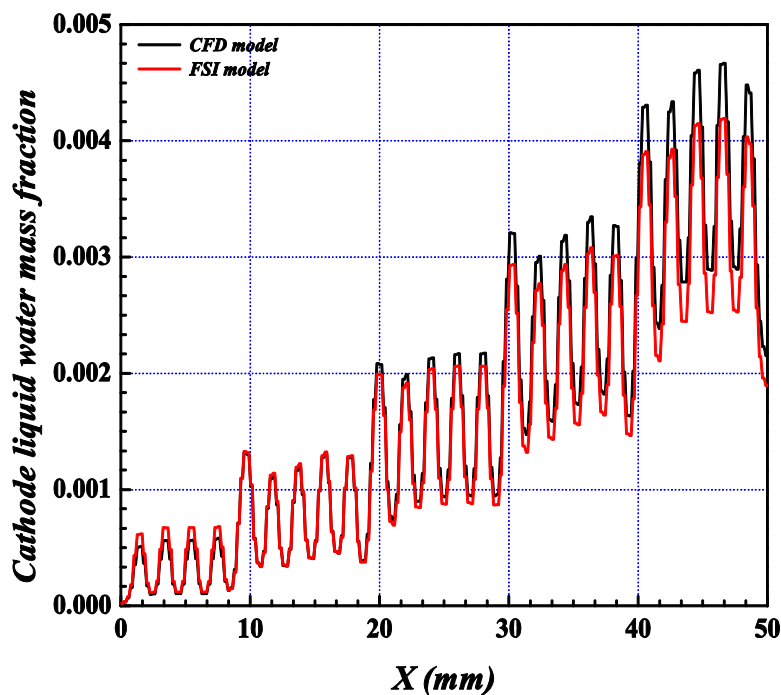
Also the membrane water content (λ) of the electrolyte membrane increases due to the water that is not discharged out of the channel, due to the drop in pressure in the channel caused by the supplied gases moving from the inlet to the outlet.

The difference in membrane water content (λ) due to the GDL deformation is $\lambda \approx 1$ in section 1, and a trade-off can be seen in section 5. This is because the liquid water decreases in section 5 due to the under-rib convection decreasing caused by the GDL compression at the under-rib. This phenomenon is repeated in the net water flux per proton (α) of Fig. 7. It can be observed that in section 1, 2 only electro-osmotic drag ($\alpha > 0$) is generated and in section 3-5 back diffusion ($\alpha < 0$) also occurs. These results match the results of the research of Springer et al. [17], who claimed that when $\lambda = 11$, back diffusion started. However, the results of the CFD model and FSI model of Fig. 7(b) show only a small difference, and there is a peculiar phenomenon in section 1-3. The width of α changes generally when the channel height changes without a change in GDL deformation [12], but when GDL deformation is included in the FSI model, α decreases, and shows a tendency to increase in the rib, and in section 4, 5 the α of the rib is shown as decreasing.

This is due to high pressure at the inlet, where there is no effect of the GDL deformation by under-rib convection, but the closer to the outlet, the pressure decreases and under-rib convection decreases. This is also shown in the Fig. 8 liquid water mass fraction, and it can be observed as having similar patterns to the results of the channel height change research of Choi et al. [12].



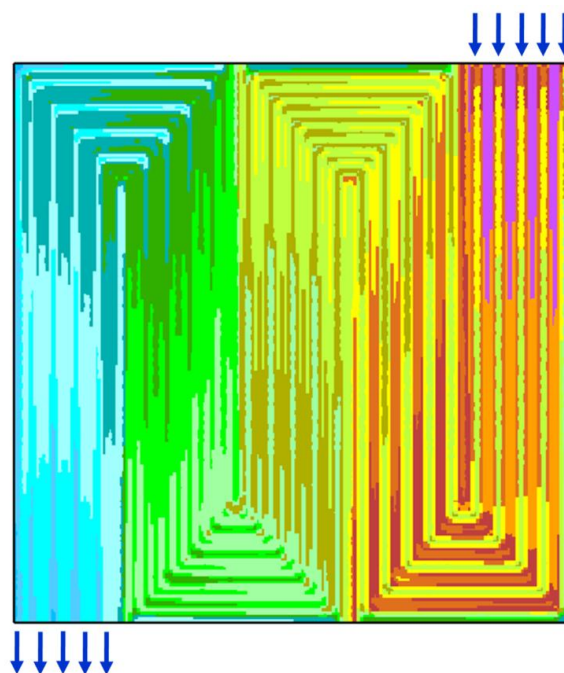
(a) Anode liquid water mass fraction



(b) Cathode liquid water mass fraction

Figure 8. Anode liquid water mass fraction and cathode liquid water mass fraction in CFD model are compared with those in FSI model at $I_{ave} = 0.6 \text{ A/cm}^2$.

The liquid water of the fuel cell is especially determined by the total pressure, membrane water content (λ), and the net water flux per proton (α), and amongst these factors the influence of the pressure is the greatest. The under-rib convection caused by the pressure difference in the channels supplies reaction gas to the rib, but also serves the role of discharging the liquid water produced by the reaction.



(a) CFD model

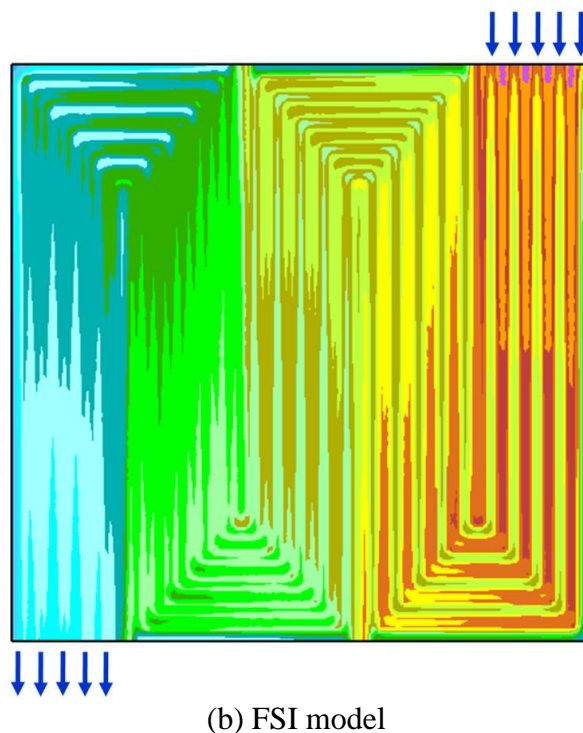


Figure 9. Current density distributions in (a) CFD model are compared with those in (b) FSI model at $I_{ave} = 0.6 \text{ A/cm}^2$.

In the case of the FSI model, as shown in Fig. 6, due to the high pressure at the inlet (section 1-2), under-rib convection can easily occur, but there is a reduction at the outlet (section 3-4). The GDL compression strain affects the gas permeability due to under-rib convection, and when comparing the $24.8 \mu\text{m}$ GDL compression deformation of the FSI model with the channel height change results of the CFD model [12], it can be predicted that the channel height will have the same results at 0.167 mm .

The movement of water in the fuel cell has a large effect on the current density distributed by the reaction area. As shown in the CFD model [12] and FSI model current density distribution in Fig 9., GDL deformation decreases under-rib convection and shows a lower current density than the CFD model, but increases as section 5 is approached. In the case of the CFD model, the gas permeability of the rib is smooth so the current density at the inlet (section 1-2) is high, but as the outlet is approached, the hydrogen and oxygen mass fractions decreases and the current density drastically decreases [12].

However, in the case of the FSI model, the cross-sectional area and the gas permeability of the rib decreases due to the GDL deformation. The decrease in cross-section area at the inlet (section 1-3) cause the internal pressure and the flow rate to increase, but the decline of the gas permeability of the rib causes low current density, and as the outlet (section 4-5) is approached, the hydrogen and oxygen mass fractions are higher than that of the CFD model, so the current density is actually increased and the current density becomes uniform overall. The increase in current density uniformity results in the fuel cell performance as shown in Fig, 10. Also as shown in λ , α of Fig. 7, the CFD model [12] and FSI model show small differences, but as the liquid water distribution largely decreases at the outlet, the FSI model, in the case of GDL deformation, is shown to be a better model in terms of fuel cell water

management, and the discharge of water is smooth resulting in an expected increase in fuel cell performance.

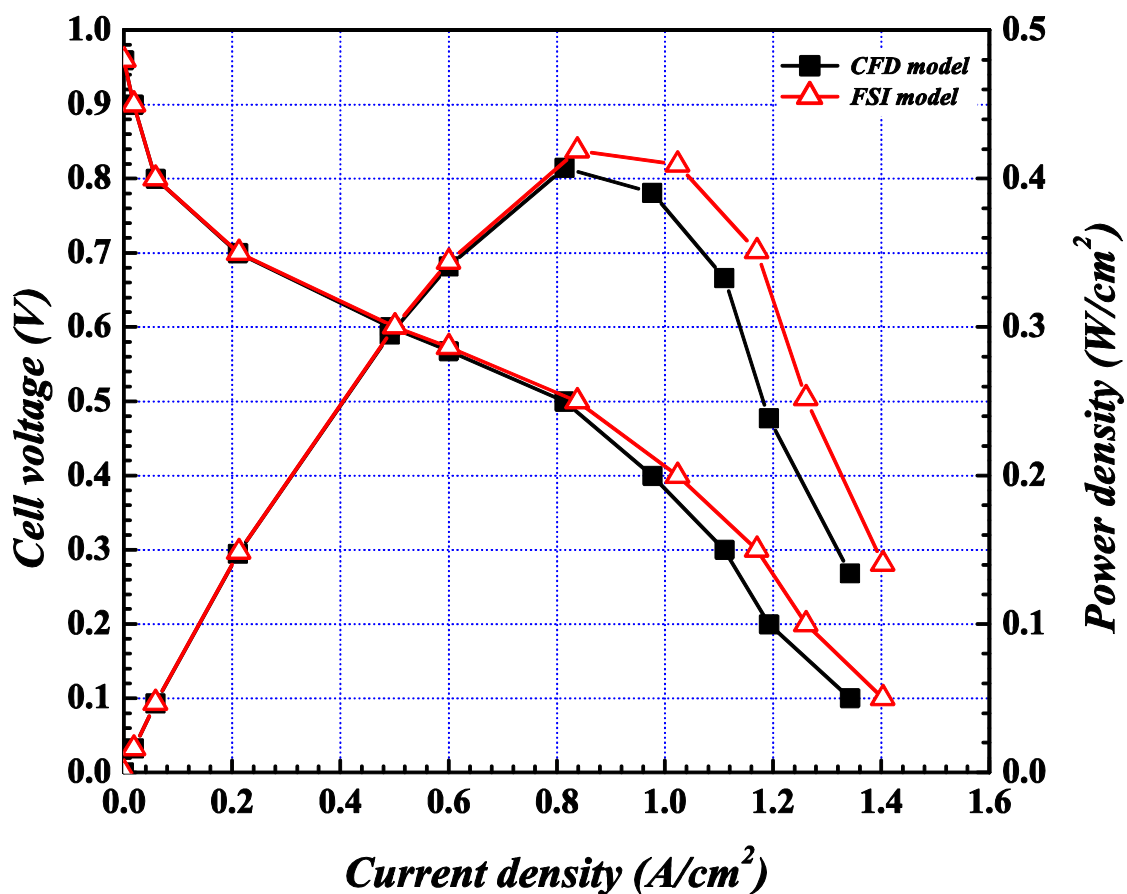


Figure 10. Comparison in polarization and power density curves between CFD model (■) and FSI model (△).

4. CONCLUSION

In this research, 5pass 4turn Serpentine flow field with a fuel cell reaction area of 25 cm² [12] was used to compare from a mass transfer point of view the CFD analysis result that does not take the GDL compression deformation into account with the FSI analysis result, that through FEA simulation takes into account GDL compression deformation.

The mechanical stress and changes that occur when assembling a fuel cell not only have a significant effect on the performance and reliability of the fuel cell, but also make the electrochemical reaction non-uniform. In the CFD model, a simple channel height change did not have a significant effect on the performance. The reason is that the reactive area of the rib and the GDL thickness are equal, so the gas permeability caused by the under-rib convection is constant.

However, in the case of the FSI model, the GDL deformation, which is caused by the decrease in gas permeability by under-rib convection, changed the flow rate, pressure drop, heat and water production etc. and also affects the amount of electric power generated by the fuel cell.

When comparing the membrane water content (λ) of the FSI model and the net water flux per proton (α) with that of the CFD model, there was only a small difference, but the total pressure, O₂/H₂ mass fraction, anode/cathode liquid water mass fraction showed a big difference.

This is due to the decrease in both the mobility of the reaction gases that move under the rib and also the mobility of the water produced, which is caused by the decrease in the channel cross sectional area and porosity being decreased by the GDL deformation. Also, although the liquid water mass fraction decreases significantly in the outlet (section 3-5), the membrane water content is not largely different from that of the CFD model, and therefore no membrane dehydration occurred, and it was confirmed that the uniformity of the current density increased.

ACKNOWLEDGEMENTS

This Research was supported by the Tongmyong University Research Grants 2013 (2013A017).

Reference

1. B. Lee, K. Park, H. M. Kim, *Int. J. Electrochem. Sci.*, 8 (2013) 219-234
2. A. P. Manso, F. F. Marzo, J. Barranco, X. Garikano, M. G. Mujika, *Int. J. Hydrogen Energy*, 37 (2012) 15256-15287
3. C. Carral, P. Mele, *Int. J. Hydrogen Energy*, 39 (2014) 4516-4530.
4. P. Zhou, C. W. Wu, *J. Power Sources*, 170 (2007) 93-100.
5. I. Taymaz, M. Benli, *Energy*, 35 (2010) 2134-2140.
6. V. Radhakrishnan, P. Haridoss, *Materials and Design*, 32 (2011) 861-868.
7. J. Kleemanna, F. Finsterwaldera, W. Tillmetz, *J. Power Sources*, 190 (2009) 92-102.
8. S. G. Kandlikar, Z. Lu, T. Y. Lin, D. Cooke, M. Daino, *J. Power Sources*, 194 (2009) 328-337.
9. S. J. Lee, C. D. Hsu, C. H. Huang, *J. Power Sources*, 145 (2005) 353-361.
10. K. Oh, P. Chippar, H. Ju, *Int. J. Hydrogen Energy*, 39 (2014) 2785-2794.
11. A. Kusoglu, A. M. Karlsson, M. H. Santare, S. Cleghorn, W. B. Johnson, *J. Power Sources*, 161 (2006) 987-996.
12. K. S. Choi, H. M. Kim, S. M. Moon, *Int. J. Hydrogen Energy*, 36 (2011) 1613-1627.
13. K. S. Choi, B. Kim, K. Park, H. M. Kim, *Computer & Fluids*, 69 (2012) 81-92.
14. ABAQUS analysis user's manual, V6.10, <http://www.3ds.com>.
15. HyperMesh Tutorial Manual: Altair Engineering, <http://www.altair.com>.
16. ES-PEMFC Methodology and Tutorial Manual: CD adapco Group, <http://www.adapco.com>
17. T. E. Springer, T. A. Zawodzinski and S. Gottesfeld, *J. Electrochem. Soc.*, 138 (1991) 2334-232.

© 2015 The Authors. Published by ESG (www.electrochemsci.org). This article is an open access article distributed under the terms and conditions of the Creative Commons Attribution license (<http://creativecommons.org/licenses/by/4.0/>).